Articles

Phase, Morphology, and Particle Size Changes Associated with the Solid−Solid Electrochemical Interconversion of TCNQ and Semiconducting CuTCNQ (TCNQ = Tetracyanoquinodimethane)

Aaron K. Neufeld,*,† Ian Madsen,‡ Alan M. Bond,*,§ and Conor F. Hogan§,||

CSIRO Manufacturing & Infrastructure Technology, P.O. Box 56 (Graham Road), Highett, Victoria 3190 Australia, CSIRO Minerals, P.O. Box 312, Clayton South, Victoria 3169, Australia, and School of Chemistry, Monash University, P.O. Box 23, Clayton, Victoria 3800, Australia

Received March 9, 2003. Revised Manuscript Received May 30, 2003

The origins of extensive solid−solid-state interconversions that accompany the electrochemistry of microparticles of tetracyanoquinodimethane (TCNQ) and semiconducting CuTCNQ (phases I and II) adhered to glassy carbon (GC) electrodes, in contact with $CuSO_{4(aq)}$ electrolyte, have been identified. Ex situ analyses with electron microscopy, infrared spectroscopy, and X-ray diffraction have been used to identify the phase changes that occur during the course of potential cycling or bulk electrolysis experiments. All redox-based transformations require extensive density, volume, and morphology changes, and consequently they are accompanied by crystal fragmentation. The net result is that extensive potential cycling ultimately leads to the thermodynamically favored TCNQ/CuTCNQ(phase II) solid−solid interconversion occurring at the nanoparticle rather than micrometer size level. The overall chemically reversible process is described by the reaction $TCNQ^0_{(S,GC)} + Cu^{2+}_{(aq)} + 2e^- \rightleftharpoons CuTCNQ_{(S,GC)}$(phase I or phase II). Needle-shaped CuTCNQ(phase I) crystals having a density of 1.80 g cm^{-3} are predominately formed in the first stages of potential cycling experiments that commence with micrometer-sized rhombic-shaped TCNQ crystals of density 1.36 g cm^{-3}. The rate of subsequent formation of thermodynamically stable CuTCNQ(phase II), which has an intermediate density of 1.66 g cm^{-3} and a crystal shape more like that of TCNQ, is dependent on the number of potential cycles, the scan rate, and the initial size of the adhered TCNQ crystals. Evidence obtained by cyclic voltametry and double potential step techniques indicate that the formation of CuTCNQ(phase I and II) involves a rate-determining nucleation and growth process, combined with the ingress and reduction of $Cu^{2+}_{(aq)}$ ions (from the electrolyte). The reactions involved in the process are believed to be $TCNQ^0_{(S,GC)} + e^- + Cu^{2+}_{(aq)} \rightleftharpoons [Cu^{2+}][TCNQ^-]_{S,GC}$ and $[Cu^{2+}][TCNQ^-]_{S,GC} + e^- \rightleftharpoons [Cu^+][TCNQ^-]_{S,GC}$ in which CuTCNQ(phase I) is formed initially and then CuTCNQ(phase II) after a large number of potential cycles. The reverse oxidation process involving the transformation of solid CuTCNQ(phases I and II) to TCNQ also involves a nucleation−growth multistep process and significant crystal size and morphology changes. Finally, data led to the postulation of a mechanism for the formation of CuTCNQ compounds via chemical reaction pathways in which the existence of the electrochemically inferred transitional $Cu^{2+}TCNQ^-_S$ intermediate also is included.

Introduction

TCNQ (7,7,8,8-tetracyanoquinodimethane, structure 1), has been characterized and studied extensively for

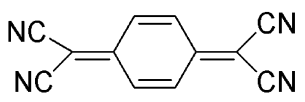

Structure 1: 7,7,8,8-tetracyanoquinodimethane, $C_{12}H_4N_4$

over 30 years.[1−6] Of particular significance, with respect to the present investigation, is the fact that TCNQ is a

* Authors to whom correspondence should be addressed. E-mails: Aaron.Neufeld@csiro.au; Alan.Bond@sci.monash.edu.au.
† CSIRO Manufacturing & Infrastructure Technology.
‡ CSIRO Minerals.
§ Monash University.
|| New address: Department of Chemistry, LaTrobe University, Victoria 3086, Australia.

(1) Long, R.; Sparks, R. *Acta Cystrallogr.* **1965**, *18*, 932−939.

10.1021/cm0341336 CCC: $25.00
Published on Web 08/21/2003

redox-active organic molecule, which, upon reduction, may be used as a component of a charge-transfer complex with conducting properties.[7−9]

The existence of charge-transfer salts was established almost immediately after TCNQ was first synthesized and applications are now common.[10−30] For example, TCNQ salts based on copper and silver have been synthesized, and these and other transition metals exhibit semiconducting properties as well as on/off switching characteristics and memory effects.[31−41]

The solid state electrochemistry of TCNQ-modified electrodes in contact with aqueous solutions of group I cations has significantly enhanced understanding of the ingress and egress of the ions required for charge neutralization.[26,27,42] On this basis, it would be envisaged that electrochemical studies aimed at elucidating the electron- and ion-transfer properties of transition metal semiconducting TCNQ compounds would be widespread. However, electrochemical studies on this class of compound have been uncommon, even though many methods of adhering microcrystals to electrode surfaces and exploring solid−solid redox-based interconversion processes are now well-developed.[43]

In the present study, the redox chemistry of solid CuTCNQ and TCNQ in the presence of aqueous $Cu^{2+}_{(aq)}$ solutions has been explored in detail using chemically modified glassy carbon (GC) electrodes. In this situation, the copper cation from the electrolyte is itself redox-active and need not be solely transported in and out of a solid TCNQ lattice for charge neutralization purposes so that the electron-transfer−charge neutralization process can be a more complex case than when group I cations are incorporated into the $TCNQ^-$ structure. Furthermore, structures 2a and 2b illustrate the different phases of CuTCNQ reported by Heintz et al.,[32]

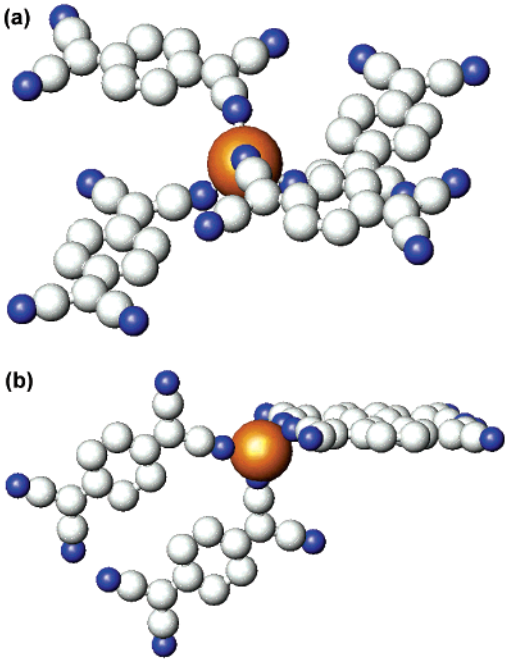

Structures 2a and 2b: Coordination of TCNQ units around the Cu atom in: (a) CuTCNQ(phase I); and (b) CuTCNQ(phase II). Nitrogen atoms in blue, carbon in white, copper in orange. Drawn with the aid of Atoms 5.1 software using data reported by Heintz *et al.*[32]

(2) Fritchie, C.; Arthur, P. *Acta Cystrallogr.* **1966**, *21*, 139−145.
(3) Lunelli, B.; Pecile, C. *J. Chem. Phys.* **1970**, *52*, 2375−2384.
(4) Hoekstra, A.; Spoelder, T.; Vos, A. *Acta Cystrallogr.* **1972**, *B28*, 14−25.
(5) Girlando, A.; Pecile, C. *Spectrochim. Acta* **1973**, *29A*, 1859−1878.
(6) Konno, M.; Saito, Y. *Acta Cystrallogr.* **1974**, *B30*, 1294−1299.
(7) Sein, L.; Wei, Y.; Jansen, S. *Synth. Met.* **2000**, *108*, 101−106.
(8) Skurski, P.; Gutowski, M. *J. Mol. Struct. (THEOCHEM)* **2000**, *531*, 339−348.
(9) Wheland, R. C.; Gillson, J. L. *J. Am. Chem. Soc.* **1976**, *98*, 3916−3925.
(10) Azcondo, M.; Ballester, L.; Golhen, S.; Gutierrez, A.; Ouahab, L.; Delhanes, P. *J. Mater. Chem.* **1999**, *9*, 1237−1244.
(11) Ballester, L.; Alonso, C.; Fonari, M.; Gutierrez, A.; Mitewa, M.; Perpinan, M.; Suwinska, K. *J. Alloys Compd.* **2001**, *323−324*, 138−141.
(12) Bozio, R.; Zanon, I.; Girlando, A.; Pecile, C. *J. Chem. Soc. Faraday Trans.* **1977**, *2*, 235−248.
(13) Campana, C.; Dunbar, K. R.; Ouyang, X. *Chem. Commun.* **1996**, 2427−2428.
(14) Fox, J.; Foxman, B.; Guarrera, D.; Miller, J.; Calabrese, J.; Reis, A. *J. Mater. Chem.* **1996**, *6*, 1627−1631.
(15) Graja, A.; Farges, J.; Brau, A.; Dupuis, P. *Synth. Met.* **1995**, *70*, 1233−1234.
(16) Hasanudin; Kuroda, N.; Sugimoto, T. *Synth. Met.* **2001**, *120*, 1045−1046.
(17) Higo, M.; Lu, X.; Mazur, U.; Hipps, K. *Thin Solid Films* **2001**, *384*, 90−101.
(18) Hooper, P.; Newton, M.; McHale, G.; Willis, M. *Semicond. Sci. Technol.* **1997**, *12*, 455−459.
(19) Khatkale, M.; Devlin, P. *J. Chem. Phys.* **1979**, *70*, 1851−1859.
(20) Kim, M.; Kim, Y.; Moon, S.; Choi, S. *Bull. Korean Chem. Soc.* **1996**, *17*, 424−428.
(21) Krysinski, P. *Adv. Mater. Opt. Electron.* **1998**, *8*, 121−128.
(22) Kunkeler, P.; Koningsbruggen, P.; Cornelissen, J.; van der Horst, A.; van der Kraan, A.; Spek, A.; Haasnoot, J.; Reedijk, J. *J. Am. Chem. Soc.* **1996**, *118*, 2190−2197.
(23) Le Cointe, M.; Lemee-Cailleau, M.; Cailleau, H.; Toudic, B. *J. Mol. Struct.* **1996**, *374*, 147−153.
(24) Miller, J.; Zhang, J.; Reiff, W.; Dixon, D.; Preston, L.; Reis, A.; Gebert, E.; Extine, M.; Troup, J.; Epstein, A.; Ward, M. *J. Phys. Chem.* **1987**, *91*, 4344−4360.
(25) Staab, H.; Weikard, J.; Ruckemann, A.; Schwogler, A. *Eur. J. Org. Chem.* **1998**, 2703−2712.
(26) Suarez, M.; Bond, A. M.; Compton, R. *J. Solid State Electrochem.* **1999**, *4*, 24−33.
(27) Symons, P. G. Ph.D. Thesis, Monash University, Melbourne, 1998; p 177.
(28) Yamaguchi, S.; Potember, R. *Synth. Met* **1996**, *78*, 117−126.
(29) Zhao, H.; Heintz, R.; Dunbar, K. R. *J. Am. Chem. Soc.* **1996**, *118*, 12844−12845.
(30) Zhao, H.; Heintz, R.; Ouyang, X.; Grandinetti, G.; Cowen, J.; Dunbar, K. R. In *Supramolecular Engineering of Synthetic Metallic Materials: Conductors and Magnets*; Kluwer: Dordrecht, 1999; pp 353−376.
(31) Azcondo, M.; Ballester, L.; Coronado, E.; Gil, A.; Gomez, C.; Gutierrez, A.; Perpinan, M.; Ramos, J.; Sanchez, A. *Synth. Met* **1997**, *86*, 1833−1834.
(32) Heintz, R. A.; Zhao, H.; Ouyang, X.; Grinetti, G.; Cowen, J.; Dunbar, K. R. *Inorg. Chem.* **1999**, *38*, 144−156.
(33) Hu, Z.; Shen, Z.; Qin, L.; Tang, S. *J. Mol. Struct.* **1995**, *356*, 163−168.
(34) Inoue, M.; Inoue, M. B. *Faraday Trans.* **1985**, *2*, 539−547.
(35) Kamitsos, E.; Tzinis, C.; Risen, W. *Solid State Commun.* **1982**, *42*, 561−565.
(36) Kaur, P.; Ballester, L.; Parmar, S.; Singh, K. *Transition Met. Chem.* **1998**, *23*, 573−576.
(37) Liu, S.; Liu, Y.; Wu, Q.; Zhu, D. *Chem. Mater.* **1996**, *8*, 2779−2787.
(38) O'Kane, S.; Clerac, R.; Zhao, H.; Ouyang, X.; Galan-Mascaros, J.; Heintz, R.; Dunbar, K. R. *J. Solid State Chem.* **2000**, *152*, 159−173.
(39) Potember, R.; Poehler, T.; Cowan, D. *Appl. Phys. Lett.* **1979**, *34*, 405−407.
(40) Potember, R.; Poehler, T.; Cowan, D.; Brant, P.; Carter, F.; Bloch, A. *Chem. Scr.* **1981**, *17*, 219−221.
(41) Yamaguchi, S.; Viands, C. A.; Potember, R. S. *J. Vac. Sci. Technol.* **1991**, *B9*, 1129−1133.
(42) Scholz, F.; Lovric, M.; Stojek, Z. *J. Solid State Electrochem.* **1997**, *1*, 134−142.
(43) Scholz, F.; Meyer, B. *Voltammetry of Solid Microparticles Immobilized on Electrode Surfaces*; Marcel Dekker Inc.: New York, 1998; Vol. 20.

either of which could be formed by electrochemical synthesis. It needs to be noted that their densities of 1.80 and 1.66 g cm^{-3}, respectively, differ significantly from each other and also from that of TCNQ (1.34 g cm^{-3}).[44] In addition, the unit cell for TCNQ is nearly twice that of either CuTCNQ(phase I or II). (The unit cell For TCNQ is 1030.86 $Å^3$, for CuTCNQ(phase I) it is 493.5 $Å^3$, and for CuTCNQ(phase II) it is 535.38 $Å^3$. (See refs 1 and 32.) Hence, large volume changes must accompany the solid−solid interconversions. Consequently, in addition to exploring the kinetics and thermodynamics of solid−solid interconversion, we have also attempted to characterize the morphology and crystal size changes that occur during the course of TCNQ/CuTCNQ(phase I or II) solid−solid transformations. Data observed by microanalysis, microscopy, X-ray diffraction, and infrared spectroscopy have been used to support our conclusions.

Experimental Section

Chemicals and Synthesis of CuTCNQ. All chemicals (analytical grade) were obtained from Aldrich, while copper disks and copper foil were obtained from Goodfellow. Stock solutions of TCNQ were prepared in acetonitrile (spectroscopic grade, Aldrich) and stored in the dark. Copper specimens (used to synthesize CuTCNQ thin films on a copper metal surface) were polished with 800 and 4000 grit SiC paper (Struers) and then cleaned in 0.5 M sulfuric acid and rinsed with ethanol prior to use. Synthesis and characterization of CuTCNQ complexes were based on procedures described by Heintz et al.[32] CuTCNQ thin films of phase I (structure 2a) were made by reaction of a clean Cu metal surface with a 10 mM TCNQ solution in acetonitrile for 1 h at room temperature (293 K), or more rapidly by dipping the Cu metal for 3 min into the same acetonitrile solution of TCNQ, now heated to 343 K. CuTCNQ thin films of phase II (structure 2b) adhered to a copper surface were made by dipping copper metal disks into an acetonitrile solution that was saturated with TCNQ for 1 h at 343 K. After reaction, the CuTCNQ(phase II) thin films were thoroughly rinsed with acetonitrile and dried under vacuum. CuTCNQ, crystals as isolated solids, were prepared by reacting CuI with TCNQ dissolved in acetonitrile for 3 min at 343 K under nitrogen. The dark blue needle-shaped crystals (phase I) were recovered by filtration, washed with acetonitrile, and then dried in a vacuum at 0.01 Pa. Conversion of phase I to phase II was performed by refluxing a suspension of phase I material in acetonitrile at 353 K for 3 h. Recovery of the phase II square-shaped crystals was the same as that for phase I needles.

Instrumentation and Procedures. Infrared (IR) spectra were obtained using a Bruker Equinox 55 spectrometer and IR Scope II infrared microscope. The IR spectra of thin films of CuTCNQ adhered to metallic copper were obtained with the aid of an inverted Praying Mantis (Harrick Scientific) diffuse reflectance optical accessory. IR spectra used to identify compounds that had formed on the surface of the glassy carbon electrode during the course of voltammetric or controlled potential electrolysis experiments were collected with the same apparatus. In these latter analyses, the electrodes to which the solid to be identified was adhered were gently immersed in distilled water after the electrochemical experiment, the excess water was removed, and the surface was dried under a stream of argon. The chemically modified electrode was then mounted in a collar to facilitate accurate downward positioning above the diffuse reflectance accessory so that the surface of the electrode was in the focal plane of the incident IR beam. Powder IR spectra of chemically synthesized CuTCNQ complexes were collected by rubbing the solid into 800 grit SiC paper (with subtraction of the background paper spectrum). In other IR experiments, a 10× reflectance objective was employed with the IR microscope. Adjustment of knife-edge apertures reduced the analysis area to approximately 100 × 100 μm in dimension.

Table 1. Band Assignments and Infrared Absorption Frequencies for CuTCNQ Compounds Prepared Chemically and Electrochemically[3,19,32,34,40]

method of preparation	ν_{50} (cm^{-1})	ν_{19} ν_{33} ν_2 (cm^{-1})	
electrolysis[a]	826	2201, 2208sh	2170
cyclic voltammetry[b]	825	2210, 2201sh	2170
copper substrate[c]	825	2201	2171
copper substrate[d]	823	2210	2172
synthesis from CuI[e]	825	2202	2171
synthesis from CuI[f]	824	2212	2171

[a] Electrolysis at 0.220 V for 15 min of $TCNQ_{(s)}$-modified GC electrode in the presence of 0.1 M $CuSO_{4(aq)}$ electrolyte. [b] Electrode conditions as for footnote *a* but after 50 cycles of the potential over the range 0.6−0.2 V at a scan rate of 0.020 V s^{-1}. [c] CuTCNQ(phase I) formed from 3-min reaction of Cu metal in 10 mM TCNQ−acetonitrile solution at 343 K. [d] CuTCNQ(phase II) formed from 70-min reaction of Cu metal in 10 mM TCNQ−acetonitrile solution at 343 K. [e] CuTCNQ(phase I) from CuI−TNCQ reaction for 3 min in acetonitrile at 343 K. [f] CuTCNQ(phase II) from CuI−TNCQ reaction for 1 h in acetonitrile at 343 K.

Electron microscopy images were obtained with a Philips XL30 field emission gun scanning electron (FEGSEM), while energy-dispersive X-ray spectra were collected using an Oxford Link EDAX system. To remove electrochemically synthesized compounds from the GC electrode, the dried surface was pressed onto double-sided carbon tape. This procedure led to solid being transferred to the carbon tape and hence to a surface that was convenient for obtaining SEM images. Microcrystals were imaged with accelerating voltages between 2 and 12 keV, using both backscatter and secondary electron detectors. Optical microscopy was achieved with an Olympus BX-51M optical microscope with 10×, 20×, and 50× magnification and the images were captured with a DM-12 digital camera. X-ray powder diffraction patterns of CuTCNQ(phase I and II) powder (obtained from metal foils or from chemical synthesis) mounted on a low-background single-crystal silicon wafer were obtained using a Philips X'Pert diffractometer equipped with a Co long fine focus tube operated at 40 kV and 40 mA. Diffraction patterns of the compounds resulting from electrolysis of $TCNQ_{(s)}$-modified indium tin oxide (ITO) electrodes in 0.1 M $CuSO_{4(aq)}$ were obtained using the same instrument. The beam path was defined using 1° divergence, 0.2-mm receiving, and 1° scatter slits. Soller slits were inserted in both the incident and diffracted beams. A curved graphite, post diffraction monochromator was used to eliminate K-beta radiation. The data were collected from 5° to 90° 2θ in steps of 0.02° with a counting time of 3.5 s $step^{-1}$.

All electrochemical measurements were carried out at 294 K using a Princeton Applied Research Model 283 potentiostat. The electrochemical cell consisted of an aqueous Ag|AgCl (3.5 M NaCl) reference electrode (Bioanalytical Systems), a platinum counter electrode, and a 1.5-mm-diameter GC working electrode (Cypress Systems). All potentials are reported as volt versus the Ag/AgCl reference electrode. Argon was used to sparge the aqueous solutions in which chemically modified GC electrodes were placed, and a flow of this gas was maintained above the solution during the course of electrochemical experiments.

TCNQ was adhered to the GC macrodisk electrode by dipping the electrode into a solution of 10 mM TCNQ in acetonitrile. The electrode was then removed from the solution and a "film" of microcrystals was formed by hanging the electrode face down and allowing the droplet of acetonitrile (containing dissolved TCNQ) to evaporate. This procedure leads to the formation of rhombus-shaped crystals with a length of between 5 and 20 μm (Figure 1a) and which are regularly spaced on the surface of the electrode. Excess TCNQ solid not in contact with the GC surface was carefully removed from the body of the electrode.

(44) Long, R.; Sparks, R.; Trueblood, K. *Acta Cystrallogr.* **1965**, *18*, 932−939.

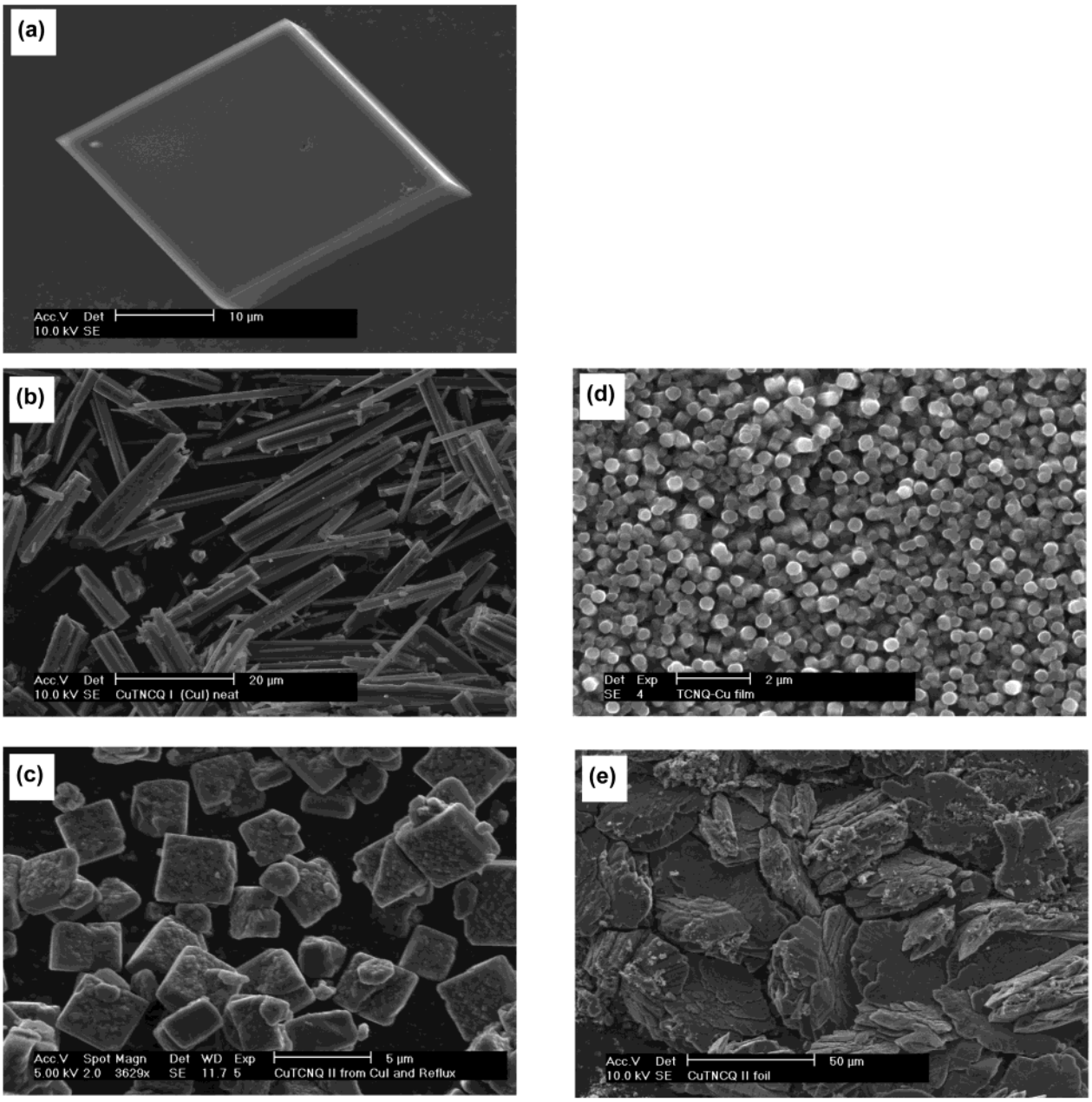

Figure 1. SEM images representative of crystals adhered to a GC electrode surface: (a) TCNQ; (b) CuTCNQ(phase I) formed by the reaction of CuI with TCNQ dissolved in hot acetonitrile; (c) CuTCNQ(phase II) formed by an extended period of reaction of CuTCNQ(phase I) with hot acetonitrile; (d) CuTCNQ(phase I); (e) phase II formed on the surface of Cu metal by the reaction of copper metal with a 10 mM TCNQ solution in acetonitrile.

Images of micrometer-sized CuTCNQ(phase I and II) crystals prepared by bulk synthesis are shown in (b) and (c) of Figure 1. Crystals prepared on copper metal surfaces (Figure 1d,e) differ significantly in size. (CuTCNQ phases formed on a copper metal surface and imaged in Figure 1d,e are top down views of the crystals. As a result, phase I needles are observed to be highly oriented normal to the surface of the copper metal from which they grew, while phase II is observed as a layered structure. Images of CuTCNQ phases shown in Figure 1b,c were obtained by transferal of crystals obtained by synthesis from CuI and TCNQ to a carbon tape. Consequently, in this case, a scattered orientation of the needlelike crystals is observed for phase I and cubic platelets for phase II.) CuTCNQ samples were adhered to the GC electrode by first dispersing the powders in a minimum amount of distilled water and then placing a small droplet on the electrode surface and allowing the water to evaporate under ambient conditions. CuTCNQ compounds formed on copper metal were first carefully removed from the surface of the copper foil or disk and then adhered to the GC electrode, as was the case with chemically synthesized CuTCNQ crystals. Small amounts of the samples used to form chemically modified electrodes were inspected by electron microscopy, X-ray diffraction, and FTIR spectroscopy to ensure the purity and identity of the compound. Data obtained on the CuTCNQ phases (Table 1) shows that the method of synthesis has very little effect on their IR spectra. For the CuTCNQ complexes, the CN stretch was centered at 2202 and 2171 cm^{-1} and 2210 and 2171 cm^{-1} for phase I and phase II, respectively. In both phases, ν_{50} was observed at about 825 cm^{-1}, thus confirming the existence of univalent TCNQ.[19] X-ray diffraction patterns for the chemically synthesized CuTCNQ(phase I and II) compounds have been provided as Supporting Information.

Results and Discussion

Voltammetry of Solid TCNQ in $CuSO_{4(aq)}$ Solutions. $Cu^{2+}_{(aq)}$ can be reduced to Cu metal at potentials

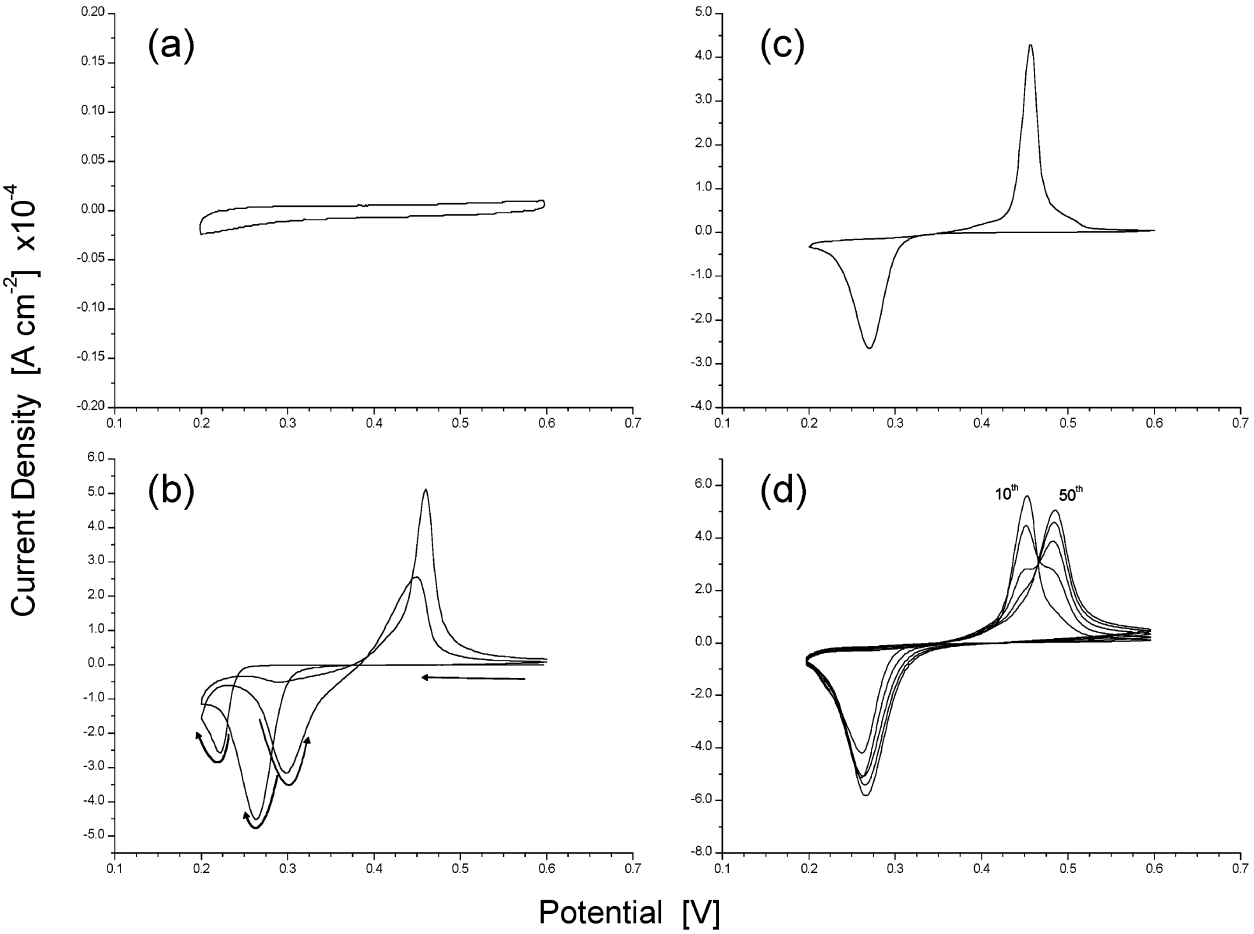

Figure 2. Cyclic voltammograms at a GC electrode in contact with 0.1 M $CuSO_{4(aq)}$ over the potential range 0.6−0.2 V at a scan rate of 0.020 V s^{-1}: (a) for an unmodified electrode; (b) the first two cycles of potential for the TCNQ-modified GC electrode where the TCNQ particle size is like that shown in Figure 1a; (c) the fifth cycle at the TCNQ-modified electrode; (d) the 10th to 50th cycle at the TCNQ-modified electrode showing every 10th cycle. The arrows indicate the sweep direction.

more negative than 0.175 V at a GC electrode. However, voltammograms for reduction of TCNQ microcrystals adhered to a GC electrode surface in contact with aqueous copper sulfate solutions can be observed because the process occurs in a potential range prior to the onset of copper deposition (Figure 2a). With TCNQ adhered to the electrode surface, cyclic voltammograms obtained for the first two cycles of the potential are extremely complex. With respect to the conditions of Figure 2b, and in the first sweep of the potential from 0.6 to 0.2 V, the onset of faradaic reduction current is detected at 0.240 V. In the course of the reverse sweep from 0.2 to 0.6 V, the current decreases initially but then again increases until a potential of 0.300 V is reached. The charge associated with a reduction on the first sweep is significantly greater than that for oxidation, implying a net accumulation of product of reduction occurs in the initial stage of the experiment. On the second sweep from 0.6 to 0.2 V, reductive faradaic current is detected at 0.300 V and continues to increase until the peak potential of 0.262 V is achieved. Subsequent cycles become more reproducible, with the magnitude of the peak currents increasing with each cycle. After five cycles of the potential (Figure 2c) the magnitude of the charge associated with the overall reduction and oxidation process is 28×10^{-5} and 26×10^{-5} C, respectively, which implies that chemical reversibility is achieved under these conditions. However, the process is far from electrochemically reversible as there is a very large gap in the peak potential for the reduction process (E_p^{red}) and for the oxidation process (E_p^{ox}) of about 0.190 V.

Furthermore, significant complexity in this process is indicated as the peak heights (I_p^{red} and I_p^{ox}) are dissimilar. In summary, voltammograms after five cycles are characterized by inert zones (an absence of significant faradaic current) when sweeping the potential in the negative direction from 0.2 to 0.6 V to until about 0.340 V, after which a sharp symmetrical peak having a half-width of about 50 mV is detected. In contrast, during the reverse potential sweep direction from 0.2 to 0.6 V, the initial inert zone is followed by a slow rise in current at 0.395 V, prior to the onset of a more asymmetric oxidation peak ($E_p^{ox} = 0.435$ V) than encountered with the reduction process. The minor process that occurs prior to this main oxidation peak may be a transient solution-based process associated with the limited solubility of a reduction product.

While Figure 2c has the appearance of a stable steady-state response, this is not the case, as evidenced by the fact that voltammograms obtained from the 10th to the 50th cycles of potential (Figure 2d) show a shift in E_p^{ox} from 0.453 to 0.485 V. The observation of an oxidation process at 0.453 V ($E_p^{ox,1}$) being replaced by one at 0.485 V ($E_p^{ox,2}$) on extended cycling of the potential suggests that slow transformation of an initially formed

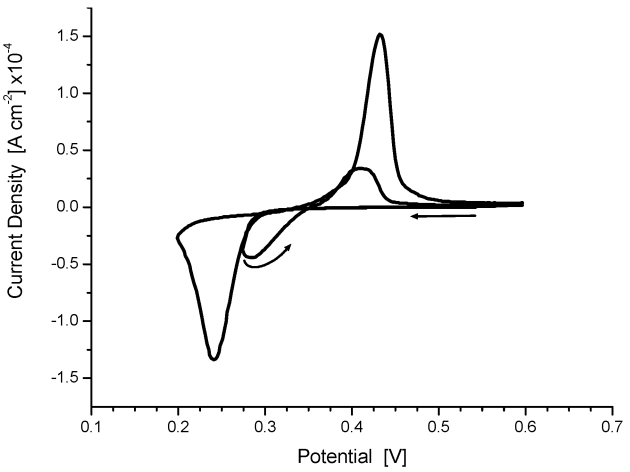

Figure 3. Cyclic voltammograms obtained at a scan rate of 0.020 V s^{-1} for a TCNQ-modified GC electrode in contact with 0.1 M $CuSO_{4(aq)}$. The initial cycle is the third cycle, which repeats a quasi-steady state. On the next (fourth) cycle, the potential is reversed at the foot of the reduction wave, which induces a hystereses loop into the voltammogram, as indicated by the arrows.

solid occurs and generates a thermodynamically more favored form of the solid.

The current loops detected in Figure 2b are indicative of nucleation and growth processes. Even more convincing evidence for the presence of this rate-determining step is contained in cyclic voltammograms switched at the onset of the reduction process and double-potential step experiments.[45,46] In the cyclic voltammogram shown in Figure 3, on the fourth cycle, the potential was switched at 0.280 V, which corresponds to the foot of the reduction process, rather than at 0.200 V, as in the preceding cycles. This protocol induces a current loop that is highly characteristic of a nucleation-growth process and also produces a zero current crossover potential of 0.361 V.

Figure 4 summarizes the results of a series of double-potential step experiments conducted on a TCNQ-modified GC electrode, which has been subjected initially to one potential cycle at a scan rate of 0.020 V s^{-1} over the potential range of 0.6−0.2 V. (This procedure was performed to "break-in" the TCNQ crystals which were freshly adhered to the GC electrode. Not performing one initial cycle of the potential necessitated the use of step potentials near the limits of the potential range, resulting in data that was not reproducible.) After each potential step, current transients show a charging current spike followed by a subsequent increase and then decrease in faradaic current over the next 2−30 s (Figure 4b,c). Again, these current−time profiles are diagnostic of the existence of a rate-determining nucleation-growth process. The magnitude of the total charge associated with reduction and oxidation (Figure 4a) is equal at 11.49×10^{-4} and 10.92×10^{-4} C, respectively, as expected for a chemically reversible process (capacitive charge subtracted). The current transients (Figure 4b,c) explicitly show that the rate of charge accumulation during both reduction and oxidation processes are directly influenced by the potential chosen for reduction only. Other experiments (data not presented) showed that the rate of charge accumulation associated with the oxidation process varied further by setting different oxidation step potentials.

A definitive structure identification of the product of reduction of $TCNQ_{(s)}$ requires analysis of single-crystal data from an X-ray diffraction measurement. In the voltametry of $TCNQ_{(s)}$ adhered to a GC electrode in contact with aqueous solutions of group I metal ions, the combined process of charge transfer and of ion insertion for charge neutralization is defined (X-ray diffraction evidence) by eq 1:[27]

$$x\mathrm{TCNQ}^{0}_{(\mathrm{S,GC})} + y\mathrm{e}^{-} + y\mathrm{M}^{+}_{(\mathrm{aq})} \rightleftharpoons (\mathrm{M}^{+})_{y}(\mathrm{TCNQ}^{-})_{y}(\mathrm{TCNQ})_{x-y\,(\mathrm{S,GC})} \quad (1)$$

In the present study, IR spectra have been primarily used to identify the formation of copper−TCNQ complexes. This approach was taken primarily due to the difficult task of obtaining diffraction patterns from the newly formed material on the surface of a GC electrode. However, in an experiment using indium tin oxide (ITO)-coated glass as the electrode material, a diffraction pattern was obtained from the electrolysis product (Figure 5). In this diffraction pattern, there are significant effects of preferred orientation of both the unreacted TCNQ and of the CuTCNQ compound, resulting in an enhancement of selected peak intensities relative to a "normal" powder pattern. Diffraction peaks observed at 12.66°, 25.48°, and 38.62° 2θ (Co Kα radiation) correspond to the (200), (400), and (600) reflections of TCNQ. The observation of these peaks, and not those from other crystallographic directions, is consistent with the morphology of TCNQ. In these samples TCNQ is present as rhombus-shaped (Figure 1a) platelets that are relatively thin along the *a* axis and hence lie flat on the substrate with the (*h*00) axis normal to the substrate. To appreciate the orientation effects, the vertical bar graph in Figure 5 shows the position and relative intensity of the powder diffraction pattern of TCNQ from the JCPDS-ICDD database (entry number 33-1899). The most intense diffractions observed by Long[44] for TCNQ are at12.64°, 21.61°, 24.94°, and 32.05° 2θ. Three of these reflections are missing from the diffraction pattern due to the fact that they are not oriented correctly to allow diffraction to occur. The diffraction peaks from electrolysis product (labeled CuTCNQ I) at 12.90°, 18.28°, and 25.96° 2θ match the powder diffraction pattern obtained from the chemically synthesized CuTCNQ(phase I). The inset in Figure 5 shows clear separation between diffraction peaks at 12.66° (TCNQ) and 12.90° (CuTCNQ phase I). In this experiment, solid TCNQ was adhered to the electrode surface in the same way as described for the GC electrode, and after the electrolysis, the electrode was rinsed with distilled water and dried in air. The electrode with both CuTCNQ and unreacted TCNQ was then subjected to a gentle rinse with acetone. This procedure assisted in reducing the intensity of diffraction originating from TCNQ by selectively dissolving it. In support of this diffraction evidence, IR spectra (Table 1) obtained from the same experiments (on both the modified GC and ITO electrode) exhibit major absorption frequencies at 2201 and 2170 cm^{-1} that closely

(45) Fletcher, S.; Halliday, C. S.; Gates, D.; Westcott, M.; Lwin, T.; Nelson, G. *J. Electroanal. Chem.* **1983**, *159*, 267−285.
(46) Armstrong, R. D.; Metcalfe, A. A. *J. Electroanal. Chem.* **1976**, *71*, 5−19.

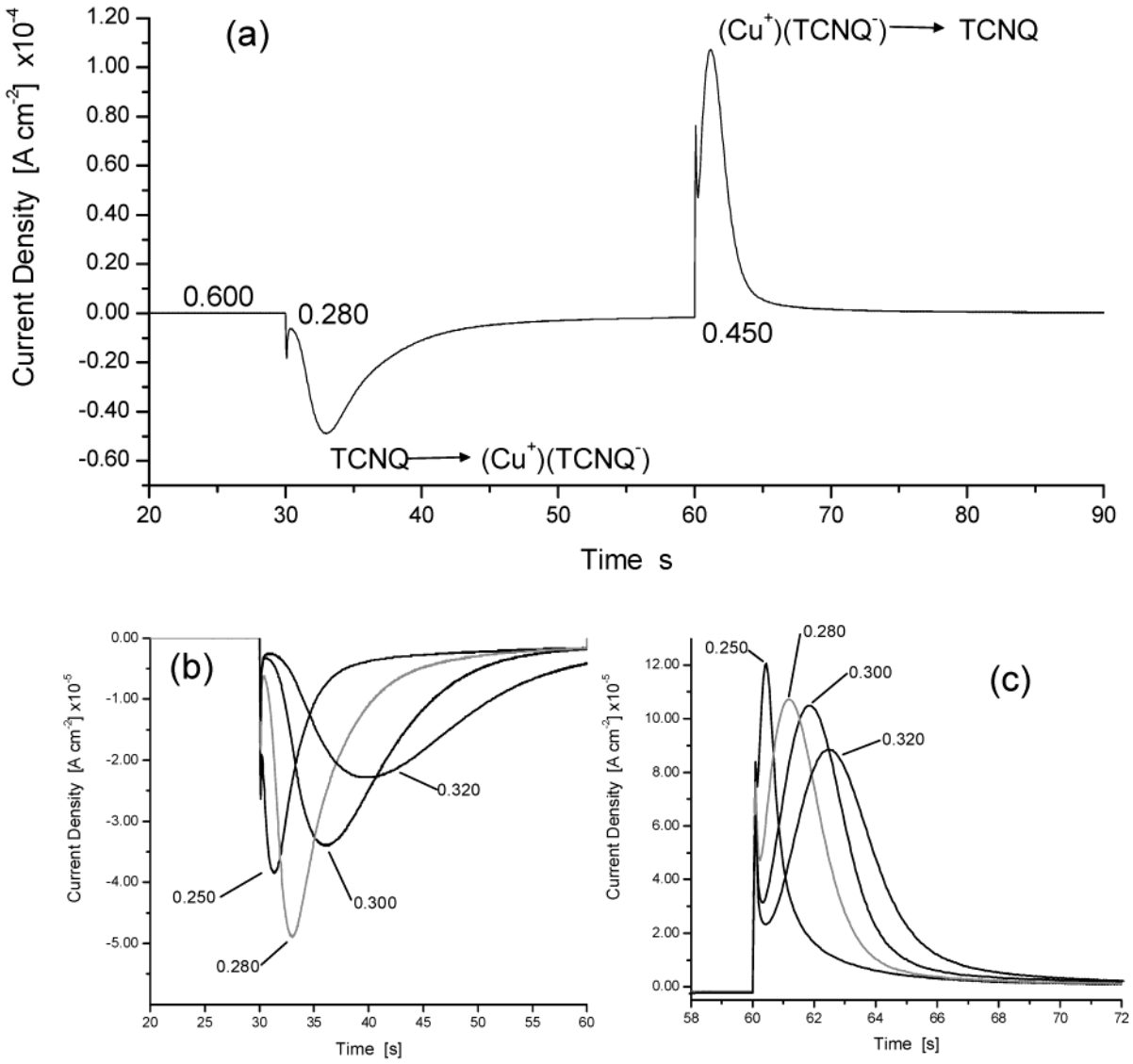

Figure 4. Double-potential step chronoamperograms for a TCNQ-modified GC electrode in contact with 0.1 M $CuSO_{4(aq)}$: (a) $I-t$ curves obtained when the potential is stepped from 0.600 to 0.280 V and then back to 0.450 V to induce the reduction and oxidation processes respectively; (b) $I-t$ curves are shown for the reduction processes when the potential is stepped from 0.600 to 0.250, 0.280, 0.300, and 0.320 V to induce reduction; (c) as for (b), but in this case $I-t$ data are displayed when the potential is stepped back to 0.450 V to induce oxidation.

resemble that obtained with an authentic CuTCNQ-(phase I) sample. However, detection of a poorly resolved shoulder at 2208 cm^{-1} implies that a small amount of CuTCNQ(phase II) also may be present.

The IR analysis of the solids formed when an excess of 50 cycles of the potential (Figure 2d) are undertaken (Table 1) exhibits a primary absorption peak centered at 2210 cm^{-1}, which is expected if CuTCNQ(phase II) is formed. A relatively small peak detected at 2223 cm^{-1} in these experiments is expected, as unreacted TCNQ also will be present. IR spectra after 5 and 50 cycles of the potential are provided as Supporting Information. Diffraction peaks from compounds formed after 50 cycles of a TCNQ-modified ITO electrode were detected for TCNQ and CuTCNQ(phase I) as described above, in addition to very weak peaks at 10.90° and 19.5° 2θ. These peaks could be attributed to CuTCNQ(phase II). It is conceivable that detection of such minute amounts of oriented crystalline compounds is beyond the capability of this conventional X-ray instrument.

The X-ray data from the ITO electrodes in combination with the IR data obtained from electrochemical experiments using GC electrodes modified with TCNQ particles (of an initial size shown in Figure 1a) imply that when TCNQ is reduced in the presence of $Cu^{2+}_{(aq)}$ electrolyte ions, CuTCNQ(phase I) is formed initially, but during the course of extensive potential cycling, CuTCNQ(phase I) is converted to the thermodynamically more stable CuTCNQ(phase II). That is, initially eq 2 applies and, after a time, eq 3 applies with solid−solid transformations involving rate-determining nucleation-growth process:

$$TCNQ^{0}_{(S,GC)} + Cu^{2+}_{(aq)} + 2e^{-} \rightleftharpoons CuTCNQ_{(S,\,GC)} \quad \text{(phase I)} \quad (2)$$

$$TCNQ^{0}_{(S,GC)} + Cu^{2+}_{(aq)} + 2e^{-} \rightleftharpoons CuTCNQ_{(S,GC)} \quad \text{(phase II)} \quad (3)$$

Intriguingly, the copper ion associated with the TCNQ complexes formed in both eqs 2 and 3 is in the univalent

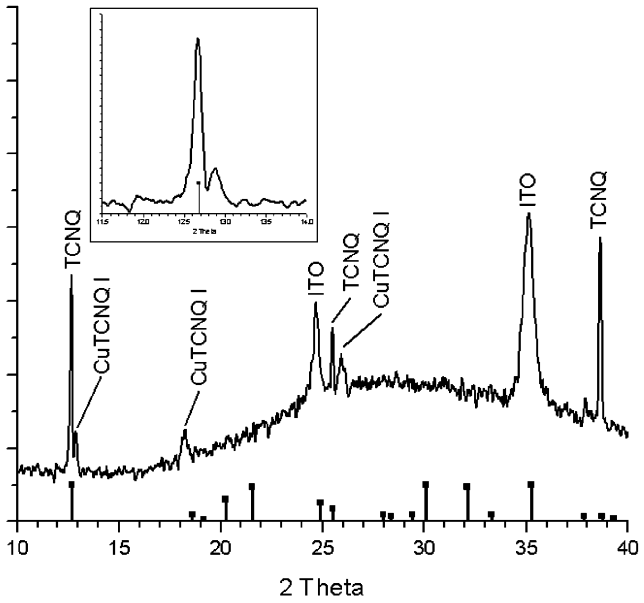

Figure 5. X-ray diffraction pattern (Co Kα) for a $TCNQ_{(s)}$-modified ITO-coated glass electrode in contact with 0.1 M $CuSO_{4(aq)}$ at a potential of 0.220 V for 15 min. Peaks corresponding to unreacted TCNQ, CuTCNQ(phase I), and indium tin oxide (ITO) are labeled. Inset: an expansion of the 2θ axis from 11.5° to 14°. The bar graph shows the position and relative intensity of a powder diffraction pattern of TCNQ.

rather than divalent oxidation state.[32,40] Hence, in this instance $Cu^{2+}_{(aq)}$ electrolyte ions are involved in both the charge neutralization and electron-transfer processes so that a significant difference exists relative to studies involving reduction of TCNQ in the presence of redox inactive electrolytes (see eq 1). However, neither the electrochemical nor IR data explain how a transitional phase I species is formed prior to the thermodynamically favored phase II. To interrogate this aspect of the problem, knowledge of the morphological changes that accompany the redox chemistry are needed.

Characterization of Morphological Changes That Accompany the Solid−Solid Electrochemical Transformations. Figure 1a provides an image of TCNQ as initially adhered to the electrode surface (almost perfect micrometer-sized crystals). Figure 6 contains electron micrographs that reveal the morphology of the CuTCNQ complex formed as a result of 15 min of reductive electrolysis at 0.220 V when TCNQ is adhered to a GC electrode in contact with 0.1 M $CuSO_{4(aq)}$. The image on the left shows the high level of fragmentation of the TCNQ crystal that occurs upon transformation to CuTCNQ(phase I). The lower magnification image on the right-hand side shows the distribution of these fractured crystals formed on the surface of the electrode. Noteworthy is the fact that because the face of the electrode was pressed into the carbon tape, the view represents that of the adhered solid that was in direct contact with the electrode surface. Clearly, the solid formed by electrolysis does not exhibit the rhombus shape of the parent TCNQ compound (Figure 1a). Close inspection of the surface of newly formed solid (Figure 7) reveals the presence of finely divided, individual needle-shaped crystals about 500 × 20 nm in dimension that are very tightly packed. This morphology is exactly that of CuTCNQ(phase I). EDAX analysis of the solid formed by reductive electrolysis confirmed the presence of Cu (Figure 7) as well as the existence of carbon and nitrogen (see Structure 2). The absence of sulfur confirms that there is no contamination from the $CuSO_{4(aq)}$ electrolyte.

Even at the highest possible magnification, SEM images of TCNQ crystals adhered to the electrode which had been in contact with 0.1 M $CuSO_{4(aq)}$ for 20 min, but in the absence of any applied potential, showed that no spontaneous transformation in the morphology occurred. Furthermore, EDAX analysis showed the absence of copper and sulfur. This control experiment revealed that the morphology changes are solely attributed to reductive electrolysis and concomitant formation of CuTCNQ(phase I).

The SEM method also can be used to elucidate the nature of the solid-state changes that accompany oxidative electrolysis of the CuTCNQ(phase I) back to TCNQ. After oxidation of CuTCNQ(phase I), the images in Figure 8 show the presence of dispersed small rhombus-shaped TCNQ crystals which are in contrast to the very much larger crystals of TCNQ initially presented (Figure 1a). In particular, the image on the right-hand side is a higher magnification micrograph that specifically illustrates the characteristic morphology of TCNQ. Clearly, the morphology of the CuTCNQ crystals formed by electrochemical reduction (identified in Figures 6 and 7) is vastly different from that of TCNQ (Figure 1a),

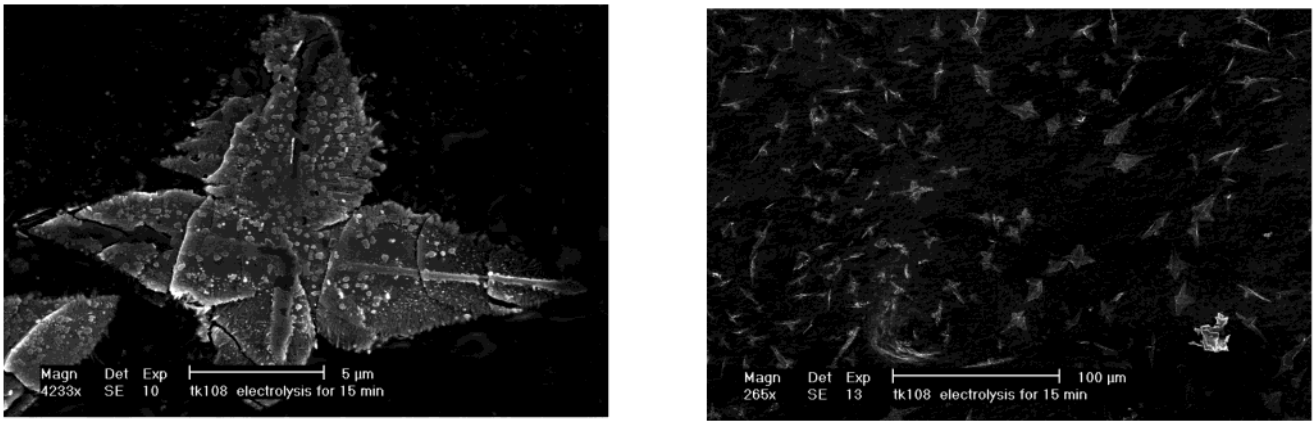

Figure 6. SEM images of CuTCNQ formed by reductive electrolysis for 20 min at 0.220 V when TCNQ adhered to GC electrode is in contact with 0.1 M $CuSO_{4(aq)}$ electrolyte: (left) a single-crystal cluster; (right) the distribution of clusters.

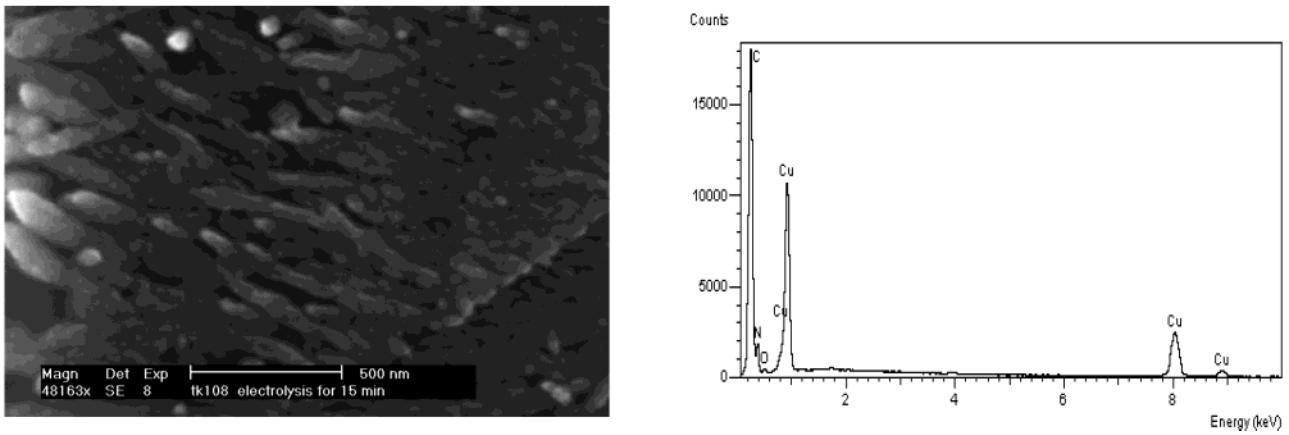

Figure 7. (Left) High-resolution image of the surface of CuTCNQ formed by reductive electrolysis of TCNQ (conditions as in Figure 6) adhered to a GC electrode in contact with 0.1 M $CuSO_{4(aq)}$ and (right) an EDAX spectrum obtained from electron microprobe analysis of this surface.

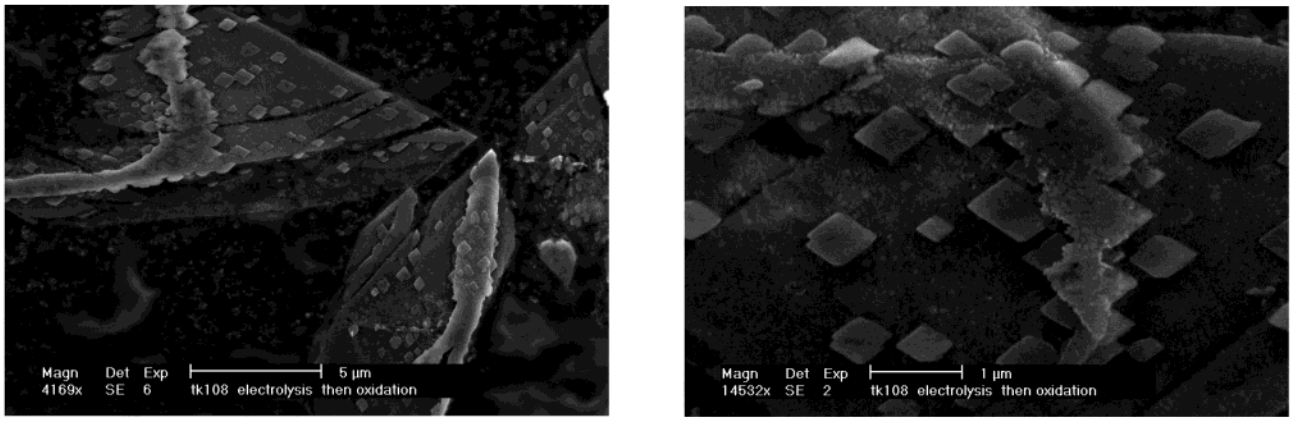

Figure 8. Images showing the formation of microcrystals of TCNQ after the sequence of reductive electrolysis of TCNQ to form CuTCNQ(phase I), followed by oxidative electrolysis of CuTCNQ when solid is adhered to a GC electrode in contact with 0.1 M $CuSO_{4(aq)}$. The left-hand image shows the morphology of a TCNQ crystal formed by this reduction−oxidation cycle. The higher magnification right-hand image shows the development of microcrystals of TCNQ, which should be compared to the crystals initially presented (see Figure 1a).

implying that the major structural changes accompany the nucleation crystal-growth steps.

The detection of drastic crystal size and morphology changes associated with electrolysis at constant potential indicated a need to identify the nature of the solid material formed on the electrode surface after potential cycling experiments. It is reasonable to assume that the large density (and volume) difference between TCNQ and CuTCNQ(phase I) of 1.34 g cm^{-3} (1030.8 $Å^3$) and 1.80 g cm^{-3} (493.5 $Å^3$), respectively, could lead to a drastic change in crystal size. To achieve these changes, crystals must fragment and become partitioned. Hence, a shift in the size distribution of electrochemically active particles toward smaller sizes occurring during each cycle of the potential may account for the shift in the oxidation peak potential noted in Figure 2d. Micrographs (Figure 9) illustrate the dominance of square-shaped platelet morphology (amidst needle-shaped crystals) after a TCNQ-modified electrode had undergone 50 potential cycles at a scan rate of 0.020 V s^{-1}. The similarity in the morphology of crystals observed after 50 cycles of the potential (Figure 9) and synthesized CuTCNQ(phase II) (Figure 1c,e) combined with the X-ray diffraction and IR data, provides convincing evidence that although CuTCNQ(phase I) is initially formed, CuTCNQ(phase II) is the dominant of the two copper complexes present upon extensive potential cycling with a TCNQ-modified electrode in the presence of $Cu^{2+}_{(aq)}$ electrolyte.

The observations of crystal size decreases on reduction of TCNQ to CuTCNQ(phase I) and during the course of oxidation back to TCNQ, in the early stages of potential cycling experiments, implies that the TCNQ/CuTCNQ-(phase II) process is only possible when very small sized crystals are adhered to the GC electrode surface. In the first cycle, TCNQ crystals are on average about 10 × 10 μm in size (Figure 1a). These are progressively altered to a dimension of less than 1 × 1 μm (Figure 8) initially, via the formation and subsequent oxidation of nanometer-sized CuTCNQ(phase I) back to TCNQ. During subsequent cycles, the dimensions of the TCNQ crystals continue to be further reduced in size until a lower size limit is achieved, which allows the formation of CuTCNQ(phase II), and hence the observation of a steady-state voltammogram involving the TCNQ/CuTCNQ(phase II) process. Formation of CuTCNQ(phase II) must therefore result from the energetically favorable solid−solid transformation from very small nanometer-sized TCNQ crystals to nanosized CuTCNQ(phase II). It is likely that the solid−solid transformation at the nanometer particle size occurs with a minimal distortion in the morphology of the crystal.

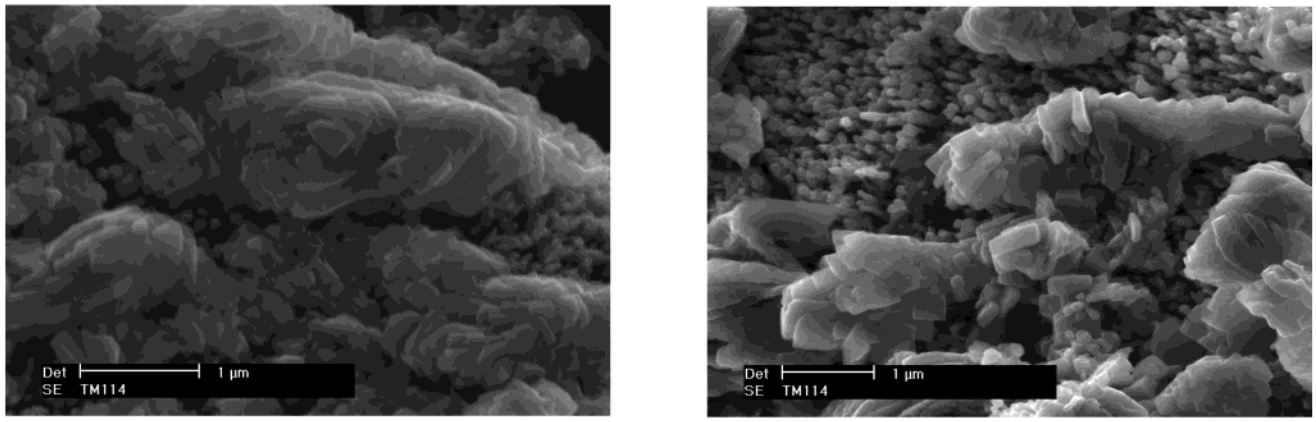

Figure 9. Images after completion of 50 cycles of the potential (0.6−0.2 V) when a TCNQ-modified GC electrode is in contact with 0.1 M $CuSO_{4(aq)}$ electrolyte. The left-hand image explicitly shows the high-density formation of sub-micrometer square-shaped crystals. The right-hand image reveals the presence of square-shaped crystals overlaying needle-shaped crystals.

Solid-State Electrochemistry of CuTCNQ Compounds. The voltametry of CuTCNQ compounds (phase I or II) adhered to a GC electrode in contact with 0.1 M $CuSO_{4(aq)}$ electrolyte, as expected, is closely related to that found with a TCNQ-modified electrode. However, some important differences are observed that are related to crystal size. In the voltammograms shown in Figure 10a, the initial potential was set at the open circuit potential with 0.1 M $CuSO4_{(aq)}$ as the electrolyte. The potential was then swept to 0.6 V at a scan rate of 0.020 V s^{-1} and then returned to the initial potential. Typically, three cycles of the potential were performed over this potential range. Under these conditions, oxidation of CuTCNQ(phase I) formed by electrolysis produced a well-defined and reproducible peak (0.462 ± 0.004 V). However, the charge associated with the voltammetric oxidation process was always significantly less (62−75%) than the charge consumed during its formation by controlled potential reductive electrolysis. This implies that a mixture of CuTCNQ(phase I) and TCNQ is present on the electrode surface under these voltammetric conditions (also consistent with data presented above). Analogous experiments conducted on CuTCNQ phases produced by the reaction of TCNQ with CuI resulted in oxidation peak potentials in the range 0.434−0.538 V (for phase I) and from 0.558 V to greater than 0.700 V for phase II. CuTCNQ phases produced from the reaction of Cu metal with dissolved TCNQ produced oxidation peak potentials in the range 0.442−0.523 V (phase I) and from 0.447 to 0.587 V (phase II). Clearly, identification of the phases by experiments of this kind is not possible as the crystal size and morphology also contributes to observed peak potentials. Representative voltammograms from these experiments when the potential is cycled in a restricted range are shown in Figure 10a.

Potential cycling experiments over the range 0.6−0.2 V when CuTCNQ phases are adhered to the GC electrode clearly lead to the formation of solid TCNQ when oxidation occurs, and hence contains features found with the solid TCNQ-modified electrode. Thus, experiments commencing with CuTCNQ(phase I) resulted in a slow decrease in I_p^{ox} of the initially detected oxidation peak ($E_p^{ox} = 0.438$ V) and the emergence of a peak ($E_p^{ox} = 0.480$ V) at more positive potentials (Figure 10b) to produce voltammograms that resemble those observed in the early stages of potential cycling (10−20 cycles) with the $TCNQ_{(s)}$-modified electrode (Figure 2d). When CuTCNQ(phase II) is adhered to the GC electrode (Figure 10c), two oxidation peaks (E_p^{ox} = 0.417 and 0.468 V) are detected, even on the first cycle, associated with residual phase II (more positive) and the formation of CuTCNQ(phase I). As expected, the peak at more positive potential (phase II) becomes dominant as the number of cycles of the potential increases. These data confirm that not all CuTCNQ is oxidized to $TCNQ_{(s)}$ and $Cu^{2+}_{(aq)}$ in a single cycle.

The data obtained with CuTCNQ confirms that the peak potentials are a function of both the size and morphology of the adhered particle, as well as the phase. Thus, oxidation of CuTCNQ(phase I or II) leads to differently sized TCNQ crystals relative to those initially present with the directly prepared TCNQ-modified electrode (Figure 1a), and the rate at which either CuTCNQ(phase I) or CuTCNQ(phase II) is formed in subsequent cycles depends on the size of the TCNQ crystal.

To confirm this conclusion, TCNQ-modified GC electrodes consisting of sub-micrometer-sized particles were prepared by rinsing the electrode with distilled water[47] before the TCNQ−acetonitrile solution on the surface had evaporated. Conversely, reapplying small droplets of TCNQ−acetonitrile solution to an upright GC electrode results in the formation of almost millimeter-sized TCNQ crystals. When performing cyclic voltametry on TCNQ-modified electrodes in the potential range 0.6−0.2 V and commencing sub-micrometer particles, the foot of the reduction peak in the first cycle commenced at 0.321 V and $E_p^{red} = 0.256$ V. On subsequent cycles (2−4), E_p^{red} was 0.263 V, with identical shapes and the quasi-steady-state TCNQ/CuTCNQ(phase I) couple being achieved after just one cycle of the potential. In contrast with 10-μm-sized particles (Figure 2b), the foot of the reduction peak on the first cycle is at 0.243 V and $E_p^{red} = 0.220$ V, and at least five cycles are required to achieve a quasi-steady state. With very large sized crystals, no faradaic current was detected up to a

(47) Hogan, C. F.; Bond, A. M.; Neufeld, A. K.; Connelly, N. G.; Llamas-Rey, E. *J. Phys. Chem. A* **2003**, *107*, 1274−1283.

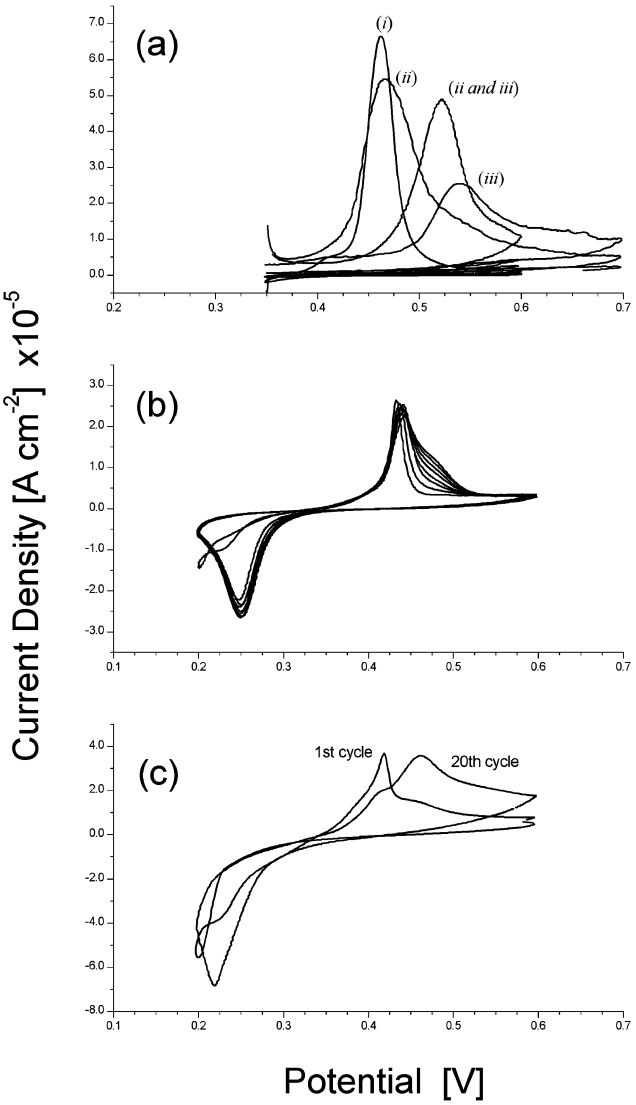

Figure 10. Voltammograms obtained at a scan rate of 0.020 V s^{-1} for CuTCNQ-modified GC electrodes in contact with 0.1 M $CuSO_{4(aq)}$: (a) oxidation of CuTCNQ(phase I and II) produced by (i) reductive electrolysis, (ii) reaction of dissolved TCNQ with CuI, and (iii) reaction of dissolved TCNQ with Cu metal; (b) potential cycling of CuTCNQ(phase I); (c) potential cycling of CuTCNQ(phase II). In (b) and (c), the formation of TCNQ microcrystals that, upon reduction, result in the initial formation of CuTCNQ(phase I) and of CuTCNQ(phase II) on subsequent cycling of the potential.

potential of 0.2 V, which confirms that the over-potential required for the nucleation and growth process is directly related to crystal size.

SEM investigations on oxidized CuTCNQ compounds also confirm the importance of the morphology. Figure 11 contains micrographs of phase I needles of the chemically synthesized CuTCNQ compound after the potential has been swept from 0.350 to 0.700 V. Oxidation leads to "etching" of the CuTCNQ crystals since phase I crystals, as synthesized, exhibit a smooth and defect-free surface when examined at even higher levels of magnification than used to obtain the images in Figure 11. Again, the drastic density and volume change that must occur when CuTCNQ(phase I) is transformed to TCNQ, and vice versa, is seen to be highly destructive to the physical nature of the crystal morphology, and simple ingress and egress of copper ions as the rate-determining step is not possible when such a mismatch of structures is required in a solid-state redox reaction.

Table 2. Voltammetric Data Obtained over the Potential Range 0.2−0.6 V at a Scan Rate of 0.020 V s^{-1} When a Modified GC Electrode in Contact with $CuSO_{4(aq)}$ Electrolyte and a TCNQ/CuTCNQ(phase I) Quasi-Steady-State Condition Has Been Achieved

$[Cu^{2+}_{(aq)}]$ (M)	E_p^{red} (V)	$W_{p,1/2}^{red}$ (V)	E_p^{ox} (V)	$W_{p,1/2}^{ox}$ (V)	E_m (V)	ΔE_p^{ox-red} (V)
1.0	0.277	0.049	0.474	0.045	0.375	0.197
0.1	0.272	0.044	0.453	0.020	0.363	0.181
0.01	0.243	0.045	0.436	0.031	0.334	0.193
0.001	0.201	0.054	0.398	0.046	0.299	0.197

Dependence of Voltametry on $CuSO_{4(aq)}$ Electrolyte Concentration. In principle, if the activities of the solids were unity, the reversible potential for the solid−solid TCNQ/CuTCNQ process could be expected to be given by the Nernst equation. If the over-potential for the oxidation and reduction processes were equal, then the midpoint potential could give the reversible potential, and this parameter, as well as E_p^{ox} and E_p^{red}, would depend on $Cu^{2+}_{(aq)}$ concentration in a Nernstian manner. However, these equilibrium-type principles do not apply to the CuTCNQ/TCNQ process. Nevertheless, the concentration of $Cu^{2+}_{(aq)}$ affects the peak position and kinetics. As discussed above, in the presence of 0.1 M $Cu^{2+}_{(aq)}$, the quasi-steady-state TCNQ/CuTCNQ(phase I) is achieved after 5 cycles of the potential at a scan rate of 0.020 V s^{-1} when commencing with crystals of the size shown in Figure 1a. In the presence of 0.01 M $CuSO_{4(aq)}$, I_p^{red} and $I_p^{ox,1}$ increase for the first 12 cycles, and $E_p^{ox,1}$ emerges as a shoulder after 12 cycles. In the presence of 0.001 M $Cu^{2+}_{(aq)}$, I_p^{red} and $I_p^{ox,1}$ increase for the first 24 cycles, and $E_p^{ox,2}$ emerges as a shoulder after 20 cycles. Quasi-steady-state voltammograms obtained at a scan rate of 0.020 V s^{-1} are shown in Figure 12 for concentrations of $Cu^{2+}_{(aq)}$ ranging from 1 M to 1 mM and the values of E_p^{red}, E_p^{ox}, the midpoint potential ($E_m = (E_p^{ox} - E_p^{red})/2$) and inert zone width ($\Delta E_p^{ox-red}$) obtained under these conditions are summarized in Table 2. The midpoint potential shifts from 0.375 V to a less positive value of 0.299 V when the $CuSO_{4(aq)}$ concentration changes from 1.0 M to 1.0 mM, which is the direction but not the magnitude expected for the change in reversible potential (predicted by a Nernst expression). This shift in E_m is a consequence of both oxidation and reduction peak potentials shifting to less positive potentials with decreasing $Cu^{2+}_{(aq)}$ concentration. In contrast, the inert zone width is almost independent of $CuSO_{4(aq)}$ concentration. Under steady-state TCNQ/CuTCNQ(phase II) conditions, $E_p^{ox,2}$ is almost independent of the $Cu^{2+}_{(aq)}$ concentration over the range 1−0.01 M, while E_p^{red} again shows a significant dependence on $Cu_{(aq)}$ concentration (Figure 12, Table 3). These $Cu^{2+}_{(aq)}$ concentration-dependent studies confirm that crystal size and morphology kinetic effects dominate thermodynamic influences of the ingress and egress of copper ions between the aqueous and solid phases.

Dependence of Voltammetry on Scan Rate. The influence of scan rate on voltammetric data is predominately on the value of E_p^{red}, which becomes less positive with faster scan rates. Negligible shifts occur in $E_p^{ox,1}$

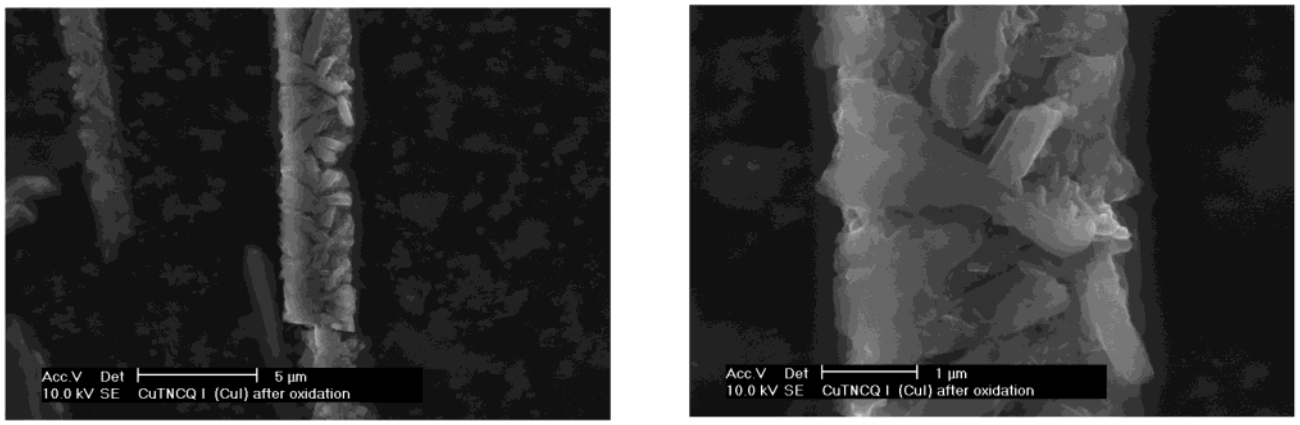

Figure 11. SEM images of crystals of CuTCNQ(phase I) after electrochemical oxidation: (left) low-resolution and (right) higher resolution images showing the "etched" crystal morphology induced by oxidative electrolysis.

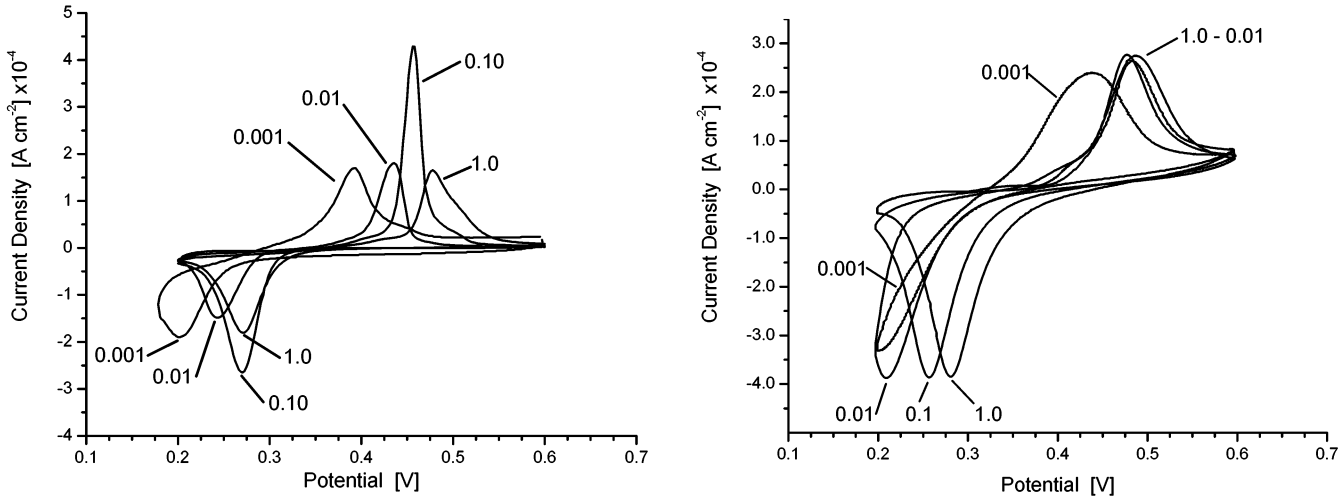

Figure 12. Voltammograms at the (left) quasi-steady state and (right) steady state obtained at a scan rate of 0.020 V s^{-1} for a TCNQ-modified GC electrode in contact with aqueous $CuSO_{4(aq)}$ electrolyte at successive concentrations.

Table 3. Voltammetric Data Obtained over the Potential Range 0.2−0.6 V at a Scan Rate of 0.020 V s^{-1} When a Modified GC Electrode in Contact with $CuSO_{4(aq)}$ Electrolyte and a TCNQ/CuTCNQ(phase II) Steady-State Condition Has Been Achieved

$[Cu^{2+}_{(aq)}]$ (M)	E_p^{red} (V)	$W_{p,1/2}^{red}$ (V)	E_p^{ox} (V)	$W_{p,1/2}^{ox}$ (V)	E_m (V)	ΔE_p^{ox-red} (V)
1.0	0.281	0.059	0.481	0.058	0.381	0.200
0.1	0.257	0.062	0.477	0.055	0.367	0.220
0.01	0.210	0.070	0.486	0.067	0.348	0.276
0.001[a]	0.200		0.437	0.097	0.318	0.237

[a] 0.1 M $Na_2SO_{4(aq)}$ supporting electrolyte added.

Table 4. Voltammetric Data Obtained as a Function of Scan Rate When a TCNQ-Modified GC Electrode Is in Contact with 0.1 M $CuSO_{4(aq)}$ Electrolyte and a TCNQ/CuTCNQ(phase I) Steady-State Condition Has Been Achieved

scan rate (V s^{-1})	E_p^{red} [a] (V)	E_p^{ox1} [a] (V)	E_p^{ox2} [a] (V)	E_{m1} [a] (V)	$\Delta E_p^{ox1-red}$ (V)	E_{m2} [a] (V)	$\Delta E_p^{ox2-red}$ (V)
0.005	0.288	0.460	0.489	0.374	0.172	0.389	0.201
0.010	0.273	0.460	0.490	0.367	0.187	0.382	0.217
0.020	0.262	0.458	0.488	0.360	0.196	0.375	0.226
0.050	0.234	0.464	0.484	0.349	0.230	0.359	0.250
0.100	0.216	0.464	0.488	0.340	0.248	0.352	0.272

[a] Volts versus Ag/AgCl.

and $E_p^{ox,2}$ (see Table 4). Consequently, changes in the midpoint potential (E_{m1}, E_{m2}) and the inert zones ($\Delta E_p^{ox1-red}$ and $\Delta E_p^{ox2-red}$) with scan rate are dominated by the E_p^{red} term.

Solids obtained from the electrode surface were analyzed by SEM after a series of experiments conducted with TCNQ adhered to a GC electrode in contact with 0.1 M $CuSO_{4(aq)}$ electrolyte when the potential was cycled (0.6−0.2 V) at a scan rate of 0.100 V s^{-1} for 5, 20, and 40 cycles and at a scan rate of 0.020 V s^{-1} for 3 and 5 cycles. At slow scan rates, there is significantly greater ingress of $Cu^{2+}_{(aq)}$ ions into the $TCNQ^-_{(s)}$ than at high scan rates, as much more of the parent TCNQ crystal has been converted to CuTCNQ(phase I) needle-like crystals even when the same experimental times are employed.

Mechanism of CuTCNQ Formation. Voltammetric data consistent with spectroscopic and microscopic evidence shows that when TCNQ is reduced in the presence of an aqueous solution of $Cu^{2+}_{(aq)}$, CuTCNQ-(phase I) is formed initially and then CuTCNQ(phase II) via an overall two-electron charge-transfer process (eqs 6a and 6b) with a nucleation-growth rate-determining step.

$$TCNQ^0_{(S,GC)} + e^- + Cu^{2+}_{(aq)} \rightleftharpoons [Cu^{2+}][TCNQ^-]_{S,GC} \quad (6a)$$

$$[Cu^{2+}][TCNQ^-]_{S,GC} + e^- \rightleftharpoons [Cu^{+}][TCNQ^-]_{S,GC} \quad (6b)$$

It is assumed in eq 6a that the transitional complex $Cu^{2+}TCNQ^{-}_{(s)}$ is formed in the solid state via transport of $Cu^{2+}_{(aq)}$ across the aqueous−solid interface in the region where direct contact of adhered $TCNQ_{(s)}$ occurs with the electrode. However, this species could transiently be in a dissolved state and then redeposit as a solid in process (6b). This could explain the existence of the small prewave accompanying the major oxidation process. When $TCNQ_{(dis)}$ reacts with $CuI_{(dis)}$ in acetonitrile (ACN) to produce $CuTCNQ_{(s)}$, it is again possible to break the process in terms of the two steps given in reactions (7a) and (7b):

$$TCNQ_{(ACN)} + Cu^{+}_{(ACN)} \rightarrow Cu^{2+}TCNQ^{-}_{(s)} \quad (7a)$$

$$Cu^{2+}TCNQ^{-}_{(s)} + I^{-}_{(ACN)} \rightarrow Cu^{+}TCNQ^{-}_{(s)} + {}^{1}/_{2}I_{2(s)} \quad (7b)$$

In this case, the transitional complex $Cu^{2+}TCNQ^{-}_{(s)}$ is reduced chemically by I^{-}, which is in turn oxidized to I_2. Finally, when TCNQ dissolved in acetonitrile comes into contact with Cu metal, the one-electron process in eq 8a can occur, followed by the reduction of the same transitional complex (8b) in previous reactions described in this section:

$$TCNQ_{(ACN)} + Cu^{0} \rightarrow Cu^{2+}TCNQ^{-}_{(s)} \quad (8a)$$

$$Cu^{2+}TCNQ^{-}_{(s)} + Cu^{0} \rightarrow Cu^{+}TCNQ^{-}_{(s)} \quad (8b)$$

In the formation of CuTCNQ from TCNQ by electrochemical or chemical means, reduction of TCNQ to $TCNQ^{-1}$ always occurs. This reaction provides a common thread for each set of reactions involving TCNQ and different oxidation states of copper.

Conclusions

The solid−solid electrochemical phase transformation of a TCNQ-modified electrode in contact with aqueous $CuSO_{4(aq)}$ electrolyte gives rise to an overall process corresponding to the reaction

$$TCNQ^{0}_{(S,GC)} + Cu^{2+}_{(aq)} + 2e^{-} \rightleftharpoons CuTCNQ_{(S,GC)} \quad \text{(phase I or phase II)}$$

The identification of CuTCNQ phases has been deduced from ex situ infrared and XRD analyses, in combination with morphological studies. Difficulty in obtaining XRD data from compounds formed in electrochemical experiments using conventional instrumentation implies that synchrotron-based analyses may be required to facilitate proper structure determinations.

Cyclic voltammograms show a complex response in the initial cycles, followed by a quasi-steady-state TCNQ/CuTCNQ(phase I) process, and finally a steady-state TCNQ/CuTCNQ(phase II) regime. Voltammograms in the quasi- and steady-state regimes show an extended inert zone width of about 0.2 V. Current hysteresis phenomena in cyclic voltammograms and data obtained by double-potential step experiments, combined with spectroscopic information, indicate that the formation of CuTCNQ(phase I or II) from $TCNQ_{(s)}$ involves both a nucleation and growth process and a reduction of $Cu^{2+}_{(aq)}$ ions rather than simple ingress of $Cu^{2+}_{(aq)}$ ions. A two-step, one-electron process, involving a transitional Cu(II)−TCNQ complex, is proposed to explain the net process.

Ex situ SEM images illustrate the physical changes that accompany this multistep transformation and reveal that micrometer-sized $TCNQ_{(s)}$ does not intercalate and accept copper ions from solution without undergoing significant morphological changes in the formation of CuTCNQ(phase I). In particular, the large density and volume change accompanying the formation of CuTCNQ(phase I) from TCNQ accounts for the highly destructive nature of the initial solid−solid transition. Formation of the thermodynamically stable CuTCNQ-(phase II) results from the existence and the reduction of nanometer-sized TCNQ crystals formed after extensive cycling of the potential. It is likely that the TCNQ/CuTCNQ(phase II) transformation does not require a significant morphological change. Voltammograms from CuTCNQ(phases I and II)-modified electrodes also indicate that a similar multistep and destructive process occurs when microcrystals of either compound are converted to sub-micrometer-sized particles of TCNQ. After extended cycling of the potential, the same behavior is observed compared to that involving TCNQ-modified electrodes where a steady-state morphology of CuTCNQ(phase II) is achieved. An apparently disproportionate amount of CuTCNQ(phase I) is always formed on the first cycle of the potential, based on SEM evidence and charge calculations. An excess of CuTCNQ(phase I) is retained for all durations of potential cycling experiments. This may be explained if some of the initially formed needle crystals become disconnected from electrical contact with the electrode surface. An equivalent excess of CuTCNQ(phase I) also may be observed when commencing experiments with chemically synthesized needle crystals that become etched (Figure 11).

The midpoint potential measured as the average of the reduction and oxidation peak potentials is a complex function of size, phase, scan rate, and $Cu^{2+}_{(aq)}$ concentration, and not a reversible potential that is directly related to the Nernst expression. The peak potential dependence on the over-potential for nucleation and growth is elucidated by purposely altering the size of crystals used to prepare the modified electrodes, where a larger crystal size is directly related to higher overpotentials.

Acknowledgment. The authors wish to thank CSIRO for funding and the facilities provided for conducting this research and N. Wright for obtaining X-ray diffraction data of the chemically synthesized CuTCNQ compounds. A. Neufeld thanks I.S. Cole of CSIRO for support during the course of this research.

Supporting Information Available: XRD powder patterns of TCNQ and CuTCNQ(phase I and II) obtained from the chemical synthesis; IR spectra of compounds adhered to the surface of a glassy carbon electrode after 5 and 50 cycles of the potential in 0.1 M $CuSO_{4(aq)}$ (PDF). This material is available free of charge via the Internet at http://pubs.acs.org.

CM0341336